The Optimal Structure−Conductivity Relation in Epoxy-Phthalocyanine Nanocomposites

L. J. Huijbregts,*,†,‡ H. B. Brom,†,‡,§ J. C. M. Brokken-Zijp,†,‡ M. Kemerink,† Z. Chen,†,‡ M. P. de Goeje,‡,|| M. Yuan,†,‡ and M. A. J. Michels†,‡

Technische Universiteit Eindhoven, P.O. Box 513, 5600 MB Eindhoven, The Netherlands, Dutch Polymer Institute (DPI), P.O. Box 902, 5600 AX Eindhoven, The Netherlands, Kamerlingh Onnes Laboratory, Leiden University, P.O. Box 9500, 2300 RA Leiden, The Netherlands, and TNO, P.O. Box 6235, 5600 HE Eindhoven, The Netherlands

Received: June 8, 2006; In Final Form: September 6, 2006

Phthalcon-11 (aquocyanophthalocyaninatocobalt (III)) forms semiconducting nanocrystals that can be dispersed in epoxy coatings to obtain a semiconducting material with a low percolation threshold. We investigated the structure−conductivity relation in this composite and the deviation from its optimal realization by combining two techniques. The real parts of the electrical conductivity of a Phthalcon-11/epoxy coating and of Phthalcon-11 powder were measured by dielectric spectroscopy as a function of frequency and temperature. Conducting atomic force microscopy (C-AFM) was applied to quantify the conductivity through the coating locally along the surface. This combination gives an excellent tool to visualize the particle network. We found that a large fraction of the crystals is organized in conducting channels of fractal building blocks. In this picture, a low percolation threshold automatically leads to a conductivity that is much lower than that of the filler. Since the structure−conductivity relation for the found network is almost optimal, a drastic increase in the conductivity of the coating cannot be achieved by changing the particle network, but only by using a filler with a higher conductivity level.

1. Introduction

Insulating polymers can be made semiconducting by adding (semi)conductive filler particles. To maintain the mechanical and processing properties of the matrix, which is preferable for applications, the filler fraction should be as low as possible, while to obtain a (semi)conductive material, the fraction should be above the critical threshold value at which the particles just form a continuous path from one side of the sample to the other. According to percolation theory, the critical filler fraction for spherical particles randomly dispersed in a matrix is 16 vol %,[1] but much lower critical filler fractions (even as low as 0.03 vol %) can and have been obtained for fillers with high aspect ratios and for fillers that form extended fractal aggregates.[2−12] Although intensive research has been done on the electrical conductivity of nanocomposites with low filler fractions, the variety of fillers that has been used is relatively small. The majority of the studies concentrate on carbon black; see, for example, refs 2−7. Other fillers that are becoming increasingly important are carbon fibers,[7,8] carbon nanotubes,[8,9] conjugated polymers,[13,14] inorganic semiconducting nanoparticles,[15] and metal particles.[16]

Nanocrystals of aquocyanophthalocyaninatocobalt (III), also called Phthalcon-11, can be used in very low amounts to make insulating thermoplastic and thermoset polymers semiconducting.[11,17] In cured epoxy coatings, the critical filler fraction (ϕ_c) of Phthalcon-11, measured along the film, decreases with increasing coating thickness, approaching a value of 0.55 vol % for bulk percolation.[12] The conductivity levels of the coatings that have been obtained are a factor $\geq 10^5$ lower than the intrinsic conductivity of Phthalcon-11. To shed light on the origin of this large difference, a detailed investigation of the relation between conductivity and composite microstructure is needed. The present paper reports on such a study, in which a range of conductivity data is compared and an analysis is made in terms of the microscopic buildup of the conductive filler network.

So far, Phthalcon-11/epoxy composites were mainly studied by four-point direct current (DC) measurements at room temperature in the Ohmic regime.[11] Measuring the conductivity as a function of frequency ($f = \omega/2\pi$), temperature (T), and electric field (E) gives more information on the morphology of the particle network and the conduction mechanism. We combined these scans with measurements of the local conduction, using conducting atomic force microscopy (C-AFM). C-AFM makes it possible to capture topographic images as well as current−voltage profiles.[18−21]

It is often assumed that the large difference between the conductivity of the nanocomposite and that of the filler is caused by insulating layers between filler particles.[22,23] However, we will show that, for the investigated cured 20 wt % (≈12 vol %) Phthalcon-11/epoxy coatings, the filler particles touch and the influence of the matrix is negligible. The difference in the conductivities of the coating and the filler can be rationalized from the structure of the particle network, in which the Phthalcon-11 nanocrystals have aggregated into fractal building blocks with a large fraction organized in conducting channels that percolate the matrix from contact to contact.

2. Experimental Section

Phthalcon-11 nanocrystals are very stable, nontoxic, nonirritating, and environment-friendly. The synthesis as described

* Corresponding author. E-mail: L.J.Huijbregst@tue.nl. Phone: + 31 40 2473059. Fax: + 31 40 2445619.
† Technische Universiteit Eindhoven.
‡ Dutch Polymer Institute (DPI).
§ Leiden University.
|| TNO.

10.1021/jp063567w CCC: $33.50
Published on Web 10/28/2006

in ref 11 provided single crystals with typical sizes of 150 nm with an aspect ratio of 0.2. They were dried for 2 days at 353 K in a vacuum oven. In the measurements of the powder conductivity, these dried crystals were used. For the preparation of Phthalcon-11/epoxy coatings, a dispersion of the dried Phthalcon-11 in *m*-cresol (Merck) was made by magnetic stirring for 1 h, followed by ultrasonic mixing for another hour, both at ambient temperature. The epoxy prepolymer (Epikote 828, Resolution Nederland BV) and the cross-linker (Jeffamine D230, Huntsman BV, Belgium) were added to this dispersion (overall NH_2/epoxy = 0.5; this is the molar ratio of the NH_2 and epoxy groups present in the prepolymer formulations). The mixture was magnetically stirred for 5 min and degassed in an ultrasonic bath for another 5 min at ambient temperature. Subsequently, the mixture was cast on 0.7 mm thick zinc substrates with a square applicator. Finally, the coatings were cured at 373 K for 4 h and postcured at 393 K for 8 h. We made two 20 wt % Phthalcon-11/epoxy coatings of 7 cm × 5 cm × 40 μm, from which several samples were cut. It was shown[11] that with this processing window no insulating top layer is formed.

The conductivity of Phthalcon-11 powder and coatings was determined by a Keithley 237 for DC measurements, whereas dielectric spectroscopy data were obtained for 40 Hz < f < 1 MHz with a Hewlett-Packard 4284A impedance meter and for 1 MHz < f < 1 GHz with an Agilent E4991A RF. The HP 4284A and the Agilent E4991A were controlled by a computer with Novocontrol software. The temperature was varied between 4 and 400 K. The holders, in which the powder was pressed by screws, had typical inner diameters of 1 cm and a height of 0.7−3 mm. The amplitude of the AC voltage was 0.1 V unless stated otherwise. Measurements and analysis of the data at frequencies higher than 1 GHz have been published elsewhere.[24] The impedance measurements on the coatings used Novocontrol sample cells with circular electrodes (a BDS 1200 and BDS 2200). We removed the coatings from the zinc substrate and evaporated 100 nm of gold on both sides of the film to decrease the contact resistance with the electrodes. When reporting AC current measurements, we mainly discuss the real part of the conductivity, $\sigma'(f)$, which is defined as $\sigma = \sigma' + i\sigma''$, where σ' and σ'' are real, $i = \sqrt{-1}$, and σ is the complex electrical conductivity, defined as $\vec{J} = \sigma\vec{E}$, with $\vec{J}$ being the current density and $\vec{E}$ being the electric field.

To visualize the microscopic current paths that run through the coating, a Digital Instruments Dimension 3100 atomic force microscope with a Nanoscope IIIa controller was combined with three different kinds of silicon cantilevers: MikroMash CSC12/Ti−Pt/4 cantilevers (Ti−Pt coating, radius of curvature ≈40 nm, spring constant ≈1.75 N/m), Olympus OMCL-AC240TM-B2 cantilevers (Pt coating, radius of curvature ≈15 nm, spring constant ≈2 N/m), and NT-MDT CSG11/Pt cantilevers (Pt coating, radius of curvature ≈35 nm, spring constant ≈0.1 N/m). The cantilevers gave similar results. The tips scanned the surface of the Phthalcon-11/epoxy coating on a zinc substrate in contact mode. In the current (I)−voltage (V) measurements, the applied voltages between the tip and zinc substrate were between 0 and 12 V. *IV* characteristics were only measured if pushing the tip harder onto the coating did not change the current.

3. Results and Discussion

3.1. Conductivity of Phthalcon-11 Powder. At room temperature, the DC conductivity (σ_{DC}) of pressed Phthalcon-11 crystallites amounts to 2 × 10^{-4} S/cm in the Ohmic regime. When corrected for the contact problems with the electrodes, the actual value of σ_{DC} will be higher by a factor 2, as estimated from the frequency and field dependence discussed below. Transfer-integral calculations based on the crystal structure suggest the in-plane conductivity to be at least 2 orders of magnitude larger than that along the *c*-axis.[25] This means that the powder conductivity will be a good measure for the in-plane conductivity of the crystals, if the crystallites are randomly distributed. Still, the value of 4 × 10^{-4} S/cm is 2 orders of magnitude lower than the conductivity (0.02 S/cm) of the Phthalcon-11 crystals as determined at 293 K by sub-THz-transmission and infrared-reflection measurements.[24] The difference hints to the presence of a less conducting surface layer either due to the difference in coordination between bulk and surface atoms of the nanocrystal or to adhesion of surface ions, like in catalysts and cluster materials.[26] A nonrandom packing of nanocrystals leading to a dominance of σ_{DC} along the *c*-axis in the powder measurements is less likely in view of $\sigma_{DC}(T)$; see below.

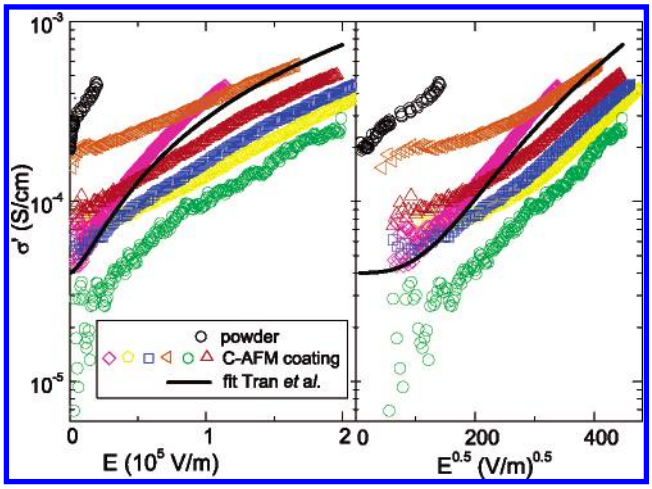

Figure 1. σ'_{DC} of Phthalcon-11 powder (black circles) and local conductivity measured with C-AFM on the coating (colored symbols) as a function of the electric field. The logarithm of σ is plotted versus E (activated behavior, panel a) and $E^{0.5}$ (panel b, see also text). The differently colored symbols are measurements on different samples and on different places within those samples. The black line is a fit according to ref 31.

The field dependence of the conductivity of Phthalcon-11 powder is shown in Figure 1. The conductivity (on a logarithmic scale) is plotted versus the electric field (E) and versus $E^{1/2}$, where straight lines correspond to theoretical expectations.[27−30] Another theoretical expectation[31] is shown as a black line and will be discussed in section 3.3. The field dependence of the conductivity of Phthalcon-11 powder shows a constant part up to a critical electric field (E_c) of 1 × 10^3 V/m. Above E_c, the conductivity has a stepwise increase by a factor of 2, similar to a step seen in the frequency scan below 1 MHz (see below). The step might be due to an increase in effective contact area. The regime of electric fields after the step is too small for a fruitful comparison with a model.

In Figure 2, $\log(\sigma')$ at 40 Hz is plotted versus $1/T^a$ ($\sigma \propto \exp[-(T_0/T)^a]$). Straight lines usually indicate Mott variable-range hopping (VRH) for $a = {}^1/_4$, hopping with a Coulomb gap or hopping in a one-dimensional system for $a = {}^1/_2$, and activated (Arrhenius) temperature dependence for $a = 1$.[32,33] Below 30 K, the measurement of the impedance (above $10^{11}\Omega$) required electric fields that are too large to remain in the Ohmic regime. From the figure, we can exclude $a = 1$. However, $a = {}^1/_2$ and $a = {}^1/_4$ both give almost straight lines, with $T_0 = 2.7 \times 10^4$ K and $T_0 = 1.1 \times 10^8$ K, respectively.

The interpretation of the value of a is not obvious. In touching semiconducting oxides such as SiO_2, the band gap will give an

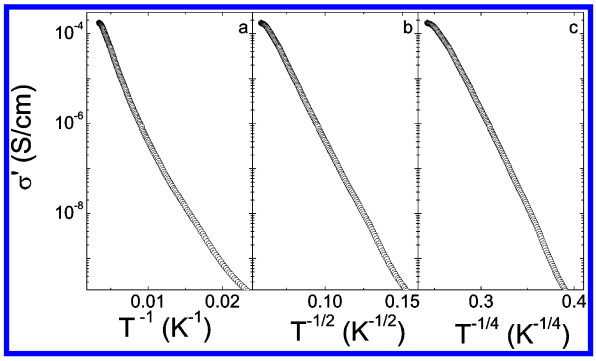

Figure 2. σ' of Phthalcon-11 powder at 40 Hz versus (a) T^{-1}, (b) $T^{-1/2}$, and (c) $T^{-1/4}$.

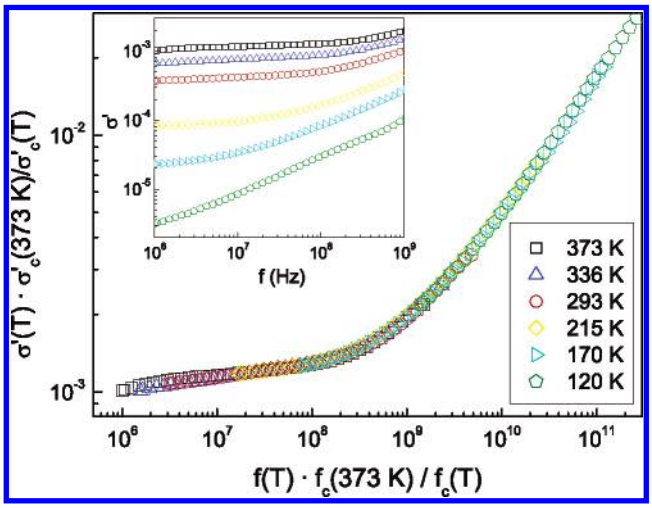

Figure 3. Master curve for frequency dependence of σ' of Phthalcon-11 powder. The inset shows the individual curves at several temperatures. When the frequency range is extended to the sub-THz regime, a value of 1.0 is approached.[24]

activated behavior for σ_{DC}, while, in granular metals or (amorphous or nanocrystalline) thin films, a value of $a = {}^1/_2$ is seen.[31,34,35] VRH in such nanocrystalline films seems to need doping states outside the nanometer sized crystals,[36] or electrostatic disorder[37] and (in)elastic cotunneling between distant resonant grains.[38] The reason for VRH in compressed pellets of relatively large (100 nm) Phthalocon-11 crystallites, for which quantum size and charging effects are less important, is not completely clear and at the moment further investigated by comparison with crystals of other sizes, but a plausible explanation is the presence of a nonconducting outer layer of the crystallites.

When measured as a function of frequency, the conductivity remained at a constant value up to 10^4 Hz. Between 10^4 and 10^6 Hz, $\sigma'(f)$ increased from 2×10^{-4} to 4×10^{-4} S/cm, followed again by an approximately constant part. The stepwise increase in conductivity between 10^4 and 10^6 Hz was not time−temperature independent in the sense that conductivity−frequency curves at different temperatures could not be brought onto one single curve as done in Figure 3. The measurements at low frequencies ($<10^4$ Hz) suffered from contact problems with the electrodes, which for $f > 10^6$ Hz are negligible (see below, discussion on master curve). For that reason, the value at 1 MHz of 4×10^{-4} S/cm will be taken as the actual DC conductivity at room temperature. The results for frequencies between 10^6 and 10^9 Hz are plotted in the inset of Figure 3.

σ' is approximately constant until a frequency of $f_c(T)$ ($f_c \approx 1 \times 10^8$ Hz at room temperature). For $f > f_c$, the conductivity increases as a function of frequency according to $\sigma'(f) \propto f^s$,

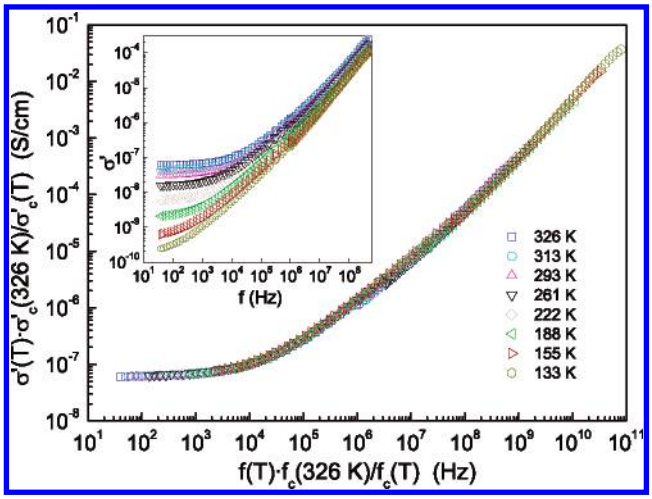

Figure 4. Master curve for frequency dependence of σ' of a Phthalcon-11/epoxy coating. The inset shows the individual curves for several temperatures.

where s slightly increases with increasing frequency and decreasing temperature. In Figure 3, s reaches a value of 0.6 at the highest frequencies and the lowest temperatures measured. However, when the frequency regime is extended, a value of 1.0 is approached.[24] This behavior is often seen in disordered materials.[39−43] The increase in conductivity originates in the presence of a network, which is not homogeneous on all length scales. At higher frequencies, the electrons travel shorter distances and therefore encounter fewer (and lower) barriers. The typical length where the inhomogeneity starts to be felt can be calculated by using the diffusion equation

$$l^2 = \sigma_{DC} k_B T/(ne^2 W_c) \qquad (1)$$

with l^2 being the mean-square nearest-neighbor distance, n the number of electrons or holes per unit volume, e the electronic charge, k_B Boltzmann's constant, and W_c the number of (nearest-neighbor) transitions per second. W_c equals $f_c/(2d)$, with d being the relevant dimension. From ref 24, we used the estimate $n \approx 10^{15}$ cm^{-3} at room temperature. The calculated length scale is found to be 0.6 μm at room temperature, which is close to the 0.45 μm found in ref 12 of a few crystals that stick together, possibly by chemical bonding.

By multiplying f with $f_c(T_{fixed})/f_c(T)$ and $\sigma'(T)$ with $\sigma'_c(T_{fixed})/\sigma'_c(T)$ (scaling of f and σ'), where T_{fixed} is a fixed temperature (373 K) and $\sigma'_c = \sigma'(f_c)$, the frequency dependence of σ' at all temperatures can be represented by one curve, the so-called master curve (Figure 3),[44] which is among others a strong indication that contact problems with the electrodes are negligible.

To sum up, the powder of Phthalcon-11 crystallites has a σ_{DC} value of 4×10^{-4} S/cm at room temperature. σ_{DC} has an E and T dependence reminiscent to variable-range hopping, while $\sigma(f)$ shows familiar scaling behavior. From the latter, a critical length scale of the order of size of a few crystals that stick together can be deduced, below which the conductivity increases beyond its DC level.

3.2. Macroscopic Conductivity of Cured Phthalcon-11/Epoxy Coatings. The inset of Figure 4 shows σ' of a 20 wt % cured Phthalcon-11/epoxy coating as a function of frequency for different temperatures. For all curves, σ' is approximately constant at low frequencies and approaches its DC value. $\sigma_{DC} = 3 \times 10^{-8}$ S/cm at room temperature, which is within a factor of 2 equal to previously reported values.[12] Above a critical

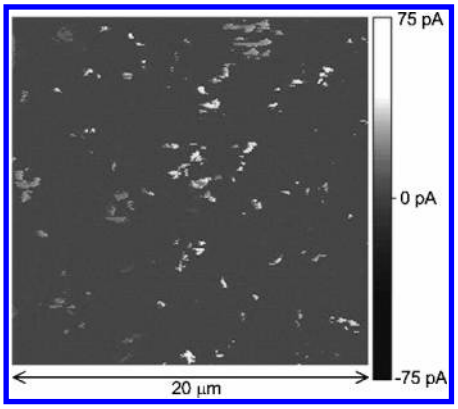

Figure 5. Current profile of an area of the Phthalcon-11/epoxy coating of 20 μm × 20 μm for a voltage of 5 V between the AFM tip and substrate. The color scale is shown on the right.

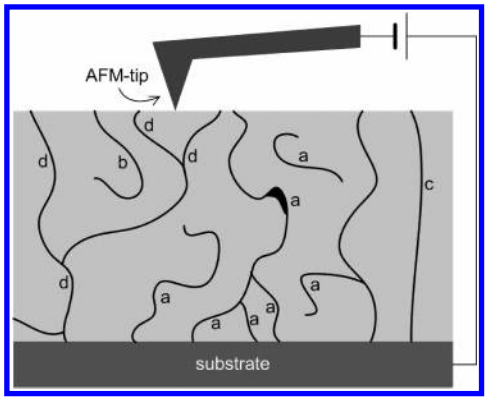

Figure 6. Illustrative sketch of the particle network inside the coating. For clarity, paths percolating in the direction parallel to the surface are not shown. For a discussion, see text.

frequency, f_c, the conductivity increases with frequency according to $\sigma' \propto f^s$, where s increases with f and decreasing T in a similar way as in the powder. The maximum value of s, at the highest frequencies and lowest temperatures measured, is 1.0. This increase in conductivity again originates in the sample inhomogeneity. Since both f_c and σ_{DC} in the coating are a factor 10^4 lower than those in the powder (the magnitudes will be discussed in a separate subsection), eq 1 gives the same typical length scale (0.5 μm, the size of some particles stuck together[12]) as found for the powder. Also, by proper scaling, a master curve can be made (see Figure 4). Like for the powder (see Figure 2), the T dependence of σ' at 40 Hz of the 20 wt % cured Phthalcon-11/epoxy coating was measured and fitted to the VRH expression. Again, a could be chosen as $^1/_2$ or $^1/_4$ and T_0 was then found to be of the same order of magnitude as that for the powder.

In short, $\sigma'(f)$ and $\sigma_{DC}(T)$ of the Phthalcon-11/epoxy coating show qualitatively the same behaviors as those for Phthalcon-11 powder, but the magnitudes of σ_{DC} and f_c are a factor of 10^4 lower. The critical length scale calculated from $\sigma'(f)$ of the coating was approximately equal to that of the filler, indicating that the contact between small groups of filler particles determines the level of DC conductivity in the composite. The question of to what extent these contacts still suffer from the presence of the ill-conducting matrix will be answered in the next two sections.

3.3. Local Conductivity of Cured Phthalcon-11/Epoxy Coatings. To find the reason for the large difference in the conductivity levels of the filler and coating, we measured the conductivity of the coating locally with C-AFM.

Figure 5 shows the current profile, measured by C-AFM, of a representative area of 20 μm × 20 μm of the Phthalcon-11/epoxy coating for a voltage of 5 V between the tip and substrate. Bright spots, corresponding to finite currents, only appear when a path of particles percolates from the surface of the coating down to the substrate. For a coating with 12 vol % particles evenly distributed, the surface fraction of particles is expected to be $(0.12)^{2/3} = 0.25$. However, in Figure 5, only 4% of the surface area conducts current. One cause might be that there are less particles near the surface than in the bulk of the coating, due to segregation by gravity or surface energies. In that case, there is an excess of particles in the bulk (see Figure 6a) that is hardly contributing to the conductivity of the coating, because the conduction at the surface of the coating forms the bottleneck. A similar effect results when there are particles at the surface that are not connected to a path percolating to the substrate (Figure 6b), so that they are not seen with C-AFM. From the 4% of the surface area contributing to the current, it can be concluded (for both reasons) that not all particles in the coating belong to ideal paths (Figure 6c) for conduction in the direction perpendicular to the surface. As the difference between the measured 4% area at the surface belonging to percolating paths and the theoretical 25% for evenly distributed particles throughout the matrix is less than an order of magnitude, the gain in conductivity for a more ideal distribution will, purely on geometrical grounds, only be modest.

It is possible to estimate the macroscopic conductivity of the coating from the AFM image (Figure 5). Assuming as a first approximation parallel conducting channels, this is done by adding the currents of all bright spots in the image and using $\sigma' = (I/V)(l/A)$ (with I being the current, V the voltage, l the length, and A the area through which the current flows). For calculating the macroscopic coating conductivity, the total area of the image ($A = 20 \times 20$ μm^2) is used and l is equal to the thickness of the coating (40 μm). Ohmic I/V values were obtained by correcting for the enhancement by the field (see next paragraph). In this way, the conductivity becomes $\sigma = 3 \times 10^{-7}$ S/cm. For 4% of the surface area linked to conducting percolating paths, this value corresponds to an average conductivity of the channels of 7×10^{-6} S/cm.

In other scans, the tip of the atomic force microscope was focused on places that would appear as bright spots in an AFM image as Figure 5 and the currents were measured as functions of the applied voltage. The conductivity was calculated with the formula above, by using the simplification that a channel of particles is a straight pile of single blocks with ribs of the order of the size of the single crystals (10^{-7} m). This leads to an area (A) of $10^{-7} \times 10^{-7}$ m^2 = 10^{-2} μm^2 and a length (l) equal to the thickness of the coating (40 μm). The conductivities in the Ohmic regime varied between 5×10^{-6} and 2×10^{-4} S/cm. The value 7×10^{-6} S/cm, calculated above, indeed falls between these two values. The field dependencies of the conductivities of several measurements with C-AFM are shown in Figure 1 together with the powder measurement. To compare the field dependence of the conductivity with existing theories, we plotted $\log(\sigma)$ versus E and $E^{1/2}$ (the straight lines in these plots correspond to the theories of refs 27 and 28 and refs 28−30, respectively) and we added in both plots a fit describing multiple cotunneling.[31,45] Since the curves of the C-AFM measurements are almost straight in both parts a and b of Figure 1 and since furthermore the fit for multiple cotunneling describes the data qualitatively as well as quantitatively very well, none of the theories can be excluded. If the theory for multiple cotunneling applies, information on the average number (j) of junctions in a row through which inelastic cotunneling takes

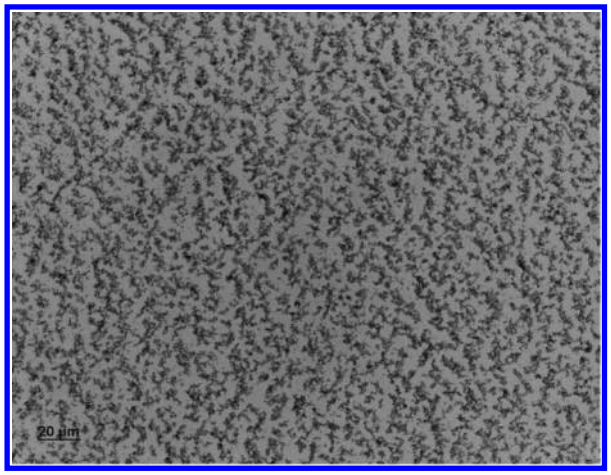

Figure 7. Optical microscope image of a 1.8 vol % Phthalcon-11/epoxy coating, taken from ref 12.

place can be obtained from the fit. The value of j was 1.75. This means that at room temperature often a virtual state of a neighboring crystal is used to reach another (next-nearest-neighbor) crystal. Moreover, it can be concluded from Figure 1 that the slope of the field dependence of the powder conductivity (after the step) is comparable to those of the channels in the coating.

The main outcome based on the C-AFM data is the prediction of $\sigma = 3 \times 10^{-7}$ S/cm for the coating, which is a factor of 10 higher than that measured with dielectric spectroscopy. $\sigma(E)$ is qualitatively similar to that of the filler material. Under the assumption of straight channels of crystals, the channel conductivity ranged from 5×10^{-6} to 2×10^{-4} S/cm.

3.4. Explanation of the Conductivity Levels. In this section, we will explain the differences in DC-conductivity levels at room temperature between the coating and the powder, measured with the various techniques.

First, we will focus on the difference between the coating conductivity measured with dielectric spectroscopy (3×10^{-8} S/cm) and the macroscopic conductivity of the coating calculated from the AFM image ($\sigma = 3 \times 10^{-7}$ S/cm). This difference is explained when several paths, which are separated at the surface, come together inside the coating (Figure 6d). The C-AFM image then gives an overestimation of the conductivity, as the currents through channels are measured one by one instead of simultaneously. To explain a factor of 10 difference, the channels of particles must have numerous branches. This is consistent with the fractal network observed by Chen et al. in their microscopic (see Figure 7) and transmission electron microscopy (TEM) images and deduced from their conductivity measurements as a function of filler fraction, which yielded a critical exponent as expected from percolation theory.[11,12]

Part of the difference between the conductivities may also be explained by the possible formation of microcracks in the films measured with dielectric spectroscopy due to the removal of the coating from the zinc substrate, leading to breaks in the particle network and thus a lower conductivity.

Second, we will consider the AFM and powder measurements. The conductivities of the channels in the coating measured with C-AFM varied between 5×10^{-6} and 2×10^{-4} S/cm. However, for the calculation, we simplified the paths of particles to straight piles of blocks. Since the structure will be more like a random percolating network, the length of the paths is actually much longer than assumed. The conductivity of the channels will therefore be higher than calculated, which will make it, at least for the channels with the highest conductivities,

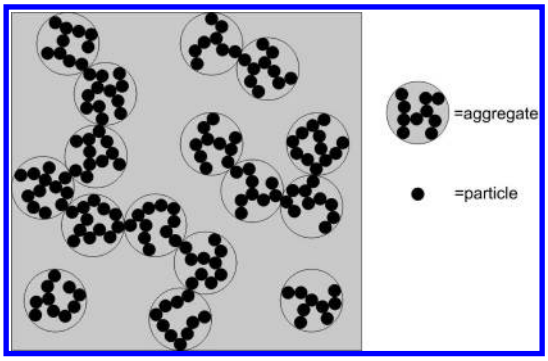

Figure 8. Schematic drawing of a random percolating network built of fractal aggregates.

comparable to the powder conductivity (4×10^{-4} S/cm). We conclude that there are channels inside the coating in which the Phthalcon-11 crystals touch: their contact is approximately as good as that in pressed powder, and the matrix does not influence the conductivity. The fact that the field and temperature dependence of the conductivities of the powder and the (channels in the) coating were similar strengthens this idea. In the channels with the lowest conductivities, the anisotropy in the particle conduction might be an important factor. Since the conductivity in one direction is expected to be a factor of 10^2 lower than in the other directions, the effect of packing in a quasi-one-dimensional channel will be much higher than that in a powder, as the current has to flow through particles stacked in the wrong direction.

We will now address the difference of a factor of 10^4 between the conductivity of the powder and that of the bulk coating. Recall that the percolation threshold of the coating in the bulk is 0.55 vol %,[12,46] appreciably below the 16 vol % for solid spheres. Such a low percolation threshold supports the picture of a more airy structure of aggregates formed during the preparation procedure.[4,11,12] In addition, we concluded in the previous paragraphs of this section that the network is fractal and that at least in a number of channels the crystals touch. Hence, we will assume that aggregates with fractal dimension (d_f) are the building blocks of a random percolating network and that inside the aggregates and between the aggregates the particles touch, as shown in Figure 8.[47] This idea, also used to explain the thickness dependence of the critical filler fraction,[12] will therefore give an upper bound for the conductivity of a nanocomposite built of fractal aggregates. The assumed structure has direct consequences for the expected saturation value of the conductivity (σ_{sat}), see Appendix A, which will be approximately the conductivity σ_a of the building block instead of the conductivity σ_p of the primary particle in that building block. This σ_a can be linked to the volume fraction of filler particles at percolation $\phi_{p,c}$ by $\sigma_a/\sigma_p = (\phi_{p,c}/0.16)^{\mu/(3-d_f)}$, with $1 + d_f/2 \leq \mu \leq 1 + d_f$. It follows from this equation that a low percolation threshold directly implies that σ_a (and therefore also the maximum conductivity of the nanocomposite, σ_{sat}) is much lower than the conductivity of the particles. Experimentally, a decreasing σ_{sat} with decreasing $\phi_{p,c}$ is generally not seen,[5,12] because the theory only gives an upper bound for the conductivity and does not take into account nonideal structures with, for example, insulating layers around the filler particles or the aggregates.

In Phthalcon-11/epoxy coatings, a fractal dimension of 1.77 $\pm$ 0.02 was measured.[12] This value supports the picture of Brownian fractal aggregates of crystals, grown during processing. This fractal dimension and a critical filler fraction of 0.55 vol %[12] give, according to eq 11, a radius of the aggregates

which is a factor of 15 larger than that of the filler particles. Notice that, strictly speaking, this model only holds for spherical particles and filler fractions up to 2.2 vol %, because, when the structure of the aggregates is independent of the filler fraction, a random close packing of aggregates at 0.64 is reached at $\phi_p = 0.022$.[48] It is experimentally observed[11,12] that $\sigma(\phi_p)$ flattens at higher filler fractions. Above 2.2 vol %, the aggregates will become denser, but apparently, this hardly influences the conductivity. We will therefore calculate the conductivity given by the model for a 2.2 vol % coating. σ of the nanocomposite is then a factor of 7×10^2 to 8×10^3 lower than σ_p, giving an upper bound for the conductivity between 5×10^{-7} and 5×10^{-8} S/cm (these boundaries are for aggregates that follow Alexander−Orbach conjecture[49] and aggregates without loops, respectively; see Appendix A). The experimental value of 3×10^{-8} S/cm differs only slightly from the theoretical upper bound for the conductivity.

4. Conclusions

By combining macroscopic conductivity measurements on a nanocomposite coating and its filler particles with local conductivity measurements on the coating, we were able to visualize the particle network inside the coating and to explain the large difference between the conductivity of the coating and that of its filler particles. The particle network is a random or almost random percolating network built of fractal aggregates. The fractal aggregates and the particles within these aggregates touch in a sufficient number of channels, as the conductivity of the percolating channels is comparable to that of pressed powder of the filler particles. The fact that the field dependence as well as the temperature dependence of the coating were similar to those of the filler particles strengthens the idea that the particles inside the coating are in good contact with each other and implies that the matrix hardly influences the conductivity inside the channels. Only a modest gain in conductivity of the coating can be expected from improvement of the contact between the particles or a more ideal distribution of fractal aggregates. It means that the structure−conductivity relation is close to optimal. For a drastic improvement of the conductivity, filler particles with a higher conductivity level have to be used. The experimental findings are shown to be in full agreement with scaling relations of percolation theory, applied to perfect fractal aggregates as the building blocks.

Appendix

A. Conduction on a Percolating Network of Fractal Building Blocks. For randomly placed conducting spheres in an insulating matrix, the following relation between the DC conductivity (σ) and the fraction (ϕ) of spheres is known from percolation theory (above the percolation threshold):[50−52]

$$\sigma = \sigma_0|\phi - \phi_c|^t \tag{2}$$

where ϕ_c is the percolation threshold ($\phi_c \approx 0.16$),[1] $t \approx 2.0$, and σ_0 is approximately equal to the conductivity of the spheres. When the building blocks of the network are fractal aggregates (denoted with subscript "a") instead of solid spheres, the equation should be written as

$$\sigma = \sigma_a|\phi_a - \phi_{a,c}|^t \tag{3}$$

with σ_a remaining to be determined and $\phi_{a,c}$ being the effective volume fraction, 0.16.

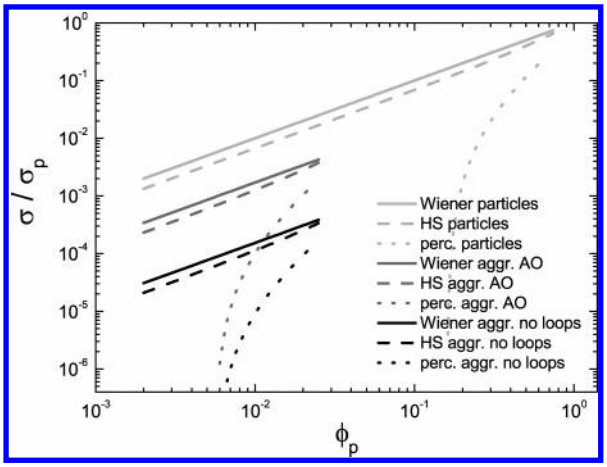

Figure 9. Upper bounds and expected value of σ (scaled by the conductivity of particles p) as a function of the volume fraction of particles embedded in a matrix with $\sigma = 0$. For the light gray lines the building blocks used in the theories are single particles, for the dark gray lines those building blocks are fractal aggregates that fulfill the Alexander−Orbach conjecture, and for the black lines they are fractal aggregates without loops. The solid lines are Wiener bounds, the dashed lines are HS bounds, and the dotted lines show the percolation theory. The lower bounds (not shown) are zero.

As σ_a and ϕ_a are not known beforehand, we want to write eq 3 in terms of σ_p and ϕ_p (where the subscript "p" stands for the particles from which the aggregates are built):

$$\sigma = \tilde{\sigma}_0|\phi_p - \phi_{p,c}|^t \tag{4}$$

To determine $\tilde{\sigma}_0$ and $\phi_{p,c}$, the following equations are used. From conservation of mass, it follows that

$$N_a m_a = N_p m_p \tag{5}$$

with N being the number and m the mass of the aggregates and particles. In addition,

$$\phi_a/\phi_p = r^3 N_a/N_p \tag{6}$$

with $r = R_a/R_p$, the ratio of the radii of the fractal aggregates and the particles, respectively. The definition of the fractal dimension (d_f) (here, d_f is the fractal dimension of the aggregates, not of the percolating network) gives

$$m_a/m_p = r^{d_f} \tag{7}$$

Elimination of N and m from eqs 5−7 yields

$$\phi_a = \phi_p r^{3-d_f} \tag{8}$$

The conductivity of the single aggregates must scale with r as well. As long as the size of the aggregate is appreciably smaller than the distance between the electrodes, the conductivity will become lower with increasing size of the aggregate (for the consequences of a relatively small distance between the electrodes see, e.g., Pollak and Hauser,[53] Raikh and Ruzin,[54] and Chen et al.[12]). It can therefore be expressed as

$$\sigma_a = \sigma_p r^{-\mu} \tag{9}$$

with μ being positive and to be determined later. Substitution of eqs 8 and 9 into eq 3 yields eq 4 with

$$\tilde{\sigma}_0 = \sigma_p r^{t(3-d_f)-\mu} \tag{10}$$

and

$$\phi_{p,c} = \phi_{a,c} r^{d_f - 3} = 0.16 r^{d_f - 3} \quad (11)$$

Elimination of r from eq 9 by using eq 11 gives the ratio between the conductivity of the aggregates and the conductivity of the particles from which they are built in terms of $\phi_{p,c}$:

$$\sigma_a/\sigma_p = (\phi_{p,c}/0.16)^{\mu/(3-d_f)} \quad (12)$$

For low $\phi_{p,c}$ and high ϕ_p, σ approaches σ_a. Therefore, eq 12 also gives the ratio between the saturation value (σ_{sat}) and σ_p.

The percolation exponent (μ) follows from the Einstein diffusion equation:[51]

$$\sigma_a \propto n_a D_a \quad (13)$$

where n_a is the charge-carrier density within the sphere of the aggregate, $n_a \propto m_a/r^3 \propto r^{d_f - 3}$, and D_a is the diffusion constant of a charge carrier, $D_a \equiv dr^2/dt$, with t being the time.[55] By defining the random-walk dimension (d_w) on a fractal as

$$r^{d_w} \propto t \quad (14)$$

it follows that

$$D_a \propto r^{2-d_w} \quad (15)$$

Substituting this, together with $n_a \propto r^{d_f - 3}$, in eq 13 yields

$$\sigma_a \propto r^{-(1+d_w-d_f)} \quad (16)$$

and thus

$$\mu = 1 + d_w - d_f \quad (17)$$

The upper bound for d_w can be found for aggregates without loops, where $l^2 \propto t$ (l is here the distance traveled by a charge carrier along an arm of the aggregate) and $l \propto r^{d_f}$, yielding $d_w = 2d_f$ and thus $\mu = 1 + d_f$, whereas for a random percolating cluster the Alexander−Orbach conjecture[49] holds, yielding $d_w = 3d_f/2$ and thus $\mu = 1 + d_f/2$.

The theory used here must predict a conductivity that is between the lower and upper bounds of other theories, like the Wiener bounds[56] and the bounds found by Hashin and Shtrikman[57] (further abbreviated as HS). This is checked in Figure 9. In the figure, only the upper bounds are shown, as the lower bounds are simply zero for a purely insulating matrix, which is assumed here. Apart from the straightforward theories for a material where phase 1 consists of particles and phase 2 is the matrix, the theories are also applied with fractal aggregates as phase 1, with the accompanying σ and ϕ given by eqs 12 and 8 (with $r = (0.16/\phi_{p,c})^{1/(3-d_f)}$, $\phi_{p,c} = 0.0055$, and $d_f = 1.77$, appropriate for the investigated Phthalcon-11/epoxy coatings). We discriminate between aggregates without loops of particles and aggregates that obey the Alexander−Orbach (AO) conjecture. Figure 9 shows that the predictions for random percolation are indeed below the accompanying upper Wiener and HS bounds.

Notice that the lines in Figure 9 are only shown until limited values of ϕ_p due to (random) maximum packing densities of the spherical particles or aggregates. ϕ_p of the 12 vol % coating is more than what theoretically can be put into the coating under the assumptions that d_f does not change with ϕ_p and that the aggregates cannot penetrate each other, because the random close packing for the aggregates of 0.64[48] corresponds to $\phi_p =$ 0.022. The theory is therefore only approximately valid for such high filler fractions.

Acknowledgment. This work forms part of the research program of the Dutch Polymer Institute (DPI), project DPI435.

Supporting Information Available: Figures showing molecular structures, a schematic representation of a Phthalcon-11 crystal, and a TEM image of Phthalcon-11 crystals. This material is available free of charge via the Internet at http://pubs.acs.org.

References and Notes

(1) Zallen, R. *The Physics of Amorphous Solids*; Wiley and Sons: New York, 1983.
(2) Brokken-Zijp, J. C. M.; Noordam, A.; Groenewoud, W. M.; Klaren, C. A. J. Patents: CA2003782, 1990; EP0370586, 1990; JP2185539, 1990.
(3) Van der Putten, D.; Moonen, J. T.; Brom, H. B.; Brokken-Zijp, J. C. M.; Michels, M. A. J. *Phys. Rev. Lett.* **1992**, *69*, 494.
(4) Adriaanse, L. J.; Reedijk, J. A.; Teunissen, P. A. A.; Brom, H. B.; Michels, M. A. J.; Brokken-Zijp, J. C. M. *Phys. Rev. Lett.* **1997**, *78*, 1755.
(5) Brokken-Zijp, J.; Soloukhin, V. A.; Posthumus, W.; De With, G. Proceedings 2003 Athens Conference on Coatings, Science and Technology, July 7−11, 2003; pp 49−69.
(6) Schueler, R.; Petermann, J.; Schulte, K.; Wentzel, H.-P. *J. Appl. Polym. Sci.* **1997**, *63*, 1741.
(7) Clingerman, M. P.; Weber, E. H.; King, J. A.; Schulz, K. H. *J. Appl. Polym. Sci.* **2003**, *88*, 2280.
(8) Flandin, L.; Verdier, M.; Boutherin, B.; Brechet, Y.; Cavaillé, J. Y. *J. Polym. Sci., Part B* **1999**, *37*, 805.
(9) Sandler, J.; Shaffer, M. S. P.; Prasse, T.; Bauhofer, W.; Schulte, K.; Windle, A. H. *Polymer* **1999**, *40*, 5967.
(10) Martin, C. A.; Sandler, J. K. W.; Shaffer, M. S. P.; Schwarz, M. K.; Bauhofer, W.; Schulte, K.; Windle, A. H. *Compos. Sci. Technol.* **2004**, *64*, 2309.
(11) Chen, Z.; Brokken-Zijp, J. C. M.; Michels, M. A. J. *J. Polym. Sci., Part B* **2006**, *44*, 33.
(12) Chen, Z.; Brokken-Zijp, J. C. M.; Huinink, H. P.; Loos, J.; De With, G.; Michels, M. A. J. *Macromolecules* **2006**, *39*, 6115.
(13) Reghu, M.; Yoon, C. O.; Yang, C. Y.; Moses, D.; Heeger, A. J.; Cao, Y. *Macromolecules* **1993**, *26*, 7245.
(14) Reghu, M.; Yoon, C. O.; Yang, C. Y.; Moses, D.; Smith, P.; Heeger, A. J.; Cao, Y. *Phys. Rev. B* **1994**, *50*, 13931.
(15) Saatweber, D.; Klostermann, P.; Rekowski, V. Patents: DE19933098-A1, 2001; WO200105897-A1, 2001; EP1216278-B1, 2005.
(16) Gonon, P.; Boudefel, A. *J. Appl. Phys.* **2006**, *99*, 024308.
(17) Brokken-Zijp, J. C. M.; De Bruijn, D. P.; Datema, K. P.; Emeis, C. A.; Kramer, A. H.; Van Mechelen, J. B.; Meruma, A. J. Patents: US05319009, EP0064254A1, WO09324562A1.
(18) Neffati, R.; Alexeev, A.; Saunin, S.; Brokken-Zijp, J. C. M.; Wouters, D.; Schmatloch, S.; Schubert, U. S.; Loos, J. *Macromol. Rapid Commun.* **2003**, *24*, 113.
(19) Shimoni, N.; Azulay, D.; Balberg, I.; Millo, O. *Phys. Status Solidi B* **2002**, *230*, 143.
(20) Azulay, D.; Eylon, M.; Eshkenazi, O.; Toker, D.; Balberg, M.; Shimoni, N.; Millo, O.; Balberg, I. *Phys. Rev. Lett.* **2003**, *90*, 236601.
(21) Kemerink, M.; Timpanaro, S.; De Kok, M. M.; Meulenkamp, E. A.; Touwslager, F. J. *J. Phys. Chem. B* **2004**, *108*, 18820.
(22) Sichel, E. K. *Carbon black-polymer composites*; Marcel Dekker, Inc.: New York, 1982.
(23) Mikrajuddin, A.; Shi, F. G.; Chungpaiboonpatana, S.; Okuyama, K.; Davidson, C.; Adams, J. M. *Mater. Sci. Semicond. Process.* **1999**, *2*, 309.
(24) Huijbregts, L. J.; Brom, H. B.; Brokken-Zijp, J. C. M.; Michels, M. A. J.; De Goeje, M. P.; Yuan, M. *Phys. Status Solidi C* **2006**, *3*, 259.
(25) Kramer, G. J.; Niele, F. G. M.; Brokken-Zijp, J. C. M. *Shell internal report* 1992.
(26) Van der Klink, J. J.; Brom, H. B. *Prog. Nucl. Magn. Reson. Spectrosc.* **2000**, *36*, 89.
(27) Pollak, M.; Riess, I. *J. Phys. C* **1976**, *9*, 2339.
(28) Fogler M. M.; Kelley, R. S. *Phys. Rev. Lett.* **2005**, *95*, 166604.
(29) Shklovskii, B. I. *Sov. Phys. Semicond.* **1976**, *10*, 855.
(30) Bourbie, D.; Ikrelef, N.; Nédellec, P. *Philos. Mag. Lett.* **2002**, *82*, 641.
(31) Tran, T. B.; Beloborodov, I. S.; Lin, X. M.; Bigioni, T. P.; Vinokur, V. M.; Jaeger, H. M. *Phys. Rev. Lett.* **2005**, *95*, 076806.
(32) Mott, N. F. *J. Non-Cryst. Solids* **1968**, *1*, 1.
(33) Shklovskii, B. I.; Efros, A. L. *Electronic Properties of Doped Semiconductors*; Springer-Verlag: Berlin, 1984.

(34) Knotek, M. L.; Pollak, M.; Donovan, T. M.; Kurtzman, M. *Phys. Rev. Lett.* **1973**, *30*, 853.
(35) Yu, D.; Wang, C.; Wehrenberg, B. L.; Guyot-Sionnest, P. *Phys. Rev. Lett.* **2004**, *92*, 216802.
(36) Zhang, J.; Shklovskii, B. I. *Phys. Rev. B* **2004**, *70*, 115317.
(37) Belodorodov, I. S.; Lopatin, A. V.; Vinokur, V. M. *Phys. Rev. B* **2000**, *72*, 125121.
(38) Feigelman, M. V.; Ioselevich, A. S. *JETP Lett.* **2005**, *81*, 277.
(39) Jonscher, A. K. *Nature (London)* **1977**, *267*, 673.
(40) Böttger, H.; Bryksin, V. V. *Hopping Conduction in Solids*; Akademie-Verlag: Berlin, 1985.
(41) Van Staveren, M. P. J.; Brom, H. B.; De Jongh, L. J. *Phys. Rep.* **1991**, *208*, 1.
(42) Dyre, J. C.; Schrøder, T. B. *Rev. Mod. Phys.* **2000**, *72*, 873.
(43) Lunkenheimer, P.; Loidl, A. *Phys. Rev. Lett.* **2003**, *91*, 207601.
(44) For Phthalcon-11 powder, the frequency can also be scaled by $\sigma_c' T$ to obtain a master curve.
(45) A constant part, corresponding to elastic cotunneling, was added to the expression for the inelastic cotunneling conductivity.
(46) For the conductivity measured perpendicular to the coating, ϕ_c will become lower than the bulk value for small thicknesses of the coating.
(47) The so-calculated critical volume fraction is an underestimate. Its value must in any case be below the percolation threshold found experimentally of 0.55 vol %.
(48) Jaeger, H. M.; Nagel, S. R. *Science* **1992**, *255*, 1524.
(49) Alexander, S.; Orbach, R. *J. Phys., Lett.* **1982**, *43*, L625.
(50) Stauffer D.; Aharony, A. *Introduction to percolation theory*; Taylor & Francis: London, 1985.
(51) Havlin, S.; Bunde, A. *Percolation II*, in *Fractals and Disordered Systems*; Bunde, A., Havlin, S., Eds.; Springer-Verlag: Berlin, 1991.
(52) Straley, J. P. *J. Phys. C* **1976**, *9*, 783; *Phys. Rev. B* **1977**, *15*, 5733.
(53) Pollak, M.; Hauser, J. J. *Phys. Rev. Lett.* **1973**, *31*, 1304.
(54) Raikh, M. E.; Ruzin, I. M. *Sov. Phys. JETP* **1987**, *65*, 1273.
(55) For convenience, we left out the brackets indicating the expectation value of r.
(56) Böttcher, C. J. F. *Theory of Electric Polarization*; Elsevier Publishing Company: Houston, TX, 1952; pp 415−420.
(57) Hashin, Z.; Shtrikman, S. *J. Appl. Phys.* **1962**, *33*, 3125.